# A Monte Carlo study of effects of chain stiffness and chain ends on dilute solution behavior of polymers. II. Second virial coefficient

AUTHOR(S):

Yamakawa, H; Yoshizaki, T

JOURNAL OF CHEMICAL PHYSICS VOLUME 119, NUMBER 2 8 JULY 2003

# A Monte Carlo study of effects of chain stiffness and chain ends on dilute solution behavior of polymers. II. Second virial coefficient

Hiromi Yamakawa and Takenao Yoshizaki
*Department of Polymer Chemistry, Kyoto University, Kyoto 606-8501, Japan*

(Received 26 February 2003; accepted 14 April 2003)

A Monte Carlo (MC) study is made of the second virial coefficient $A_2$ for polymers using two freely rotating chains, each of bond angle 109°, with the Lennard-Jones 6-12 intramolecular and intermolecular potentials between beads in a cutoff version for the number of bonds in the chain ranging from 6 to 1000 in the $\Theta$ and good-solvent conditions. It is found that effects of chain ends on $A_2$ are appreciable for small molecular weight $M$, as was expected, and that the second virial coefficient $A_{2,\Theta}$ at the $\Theta$ temperature, at which the ratio $\langle S^2\rangle/M$ of the mean-square radius of gyration $\langle S^2\rangle$ to $M$ becomes a constant independent of $M$ for very large $M$, remains slightly negative even for such large (but finite) $M$ where the effects of chain ends disappear. Such behavior of $A_{2,\Theta}$, which cannot be explained within the framework of the binary cluster theory, is shown to be understandable if possible effects of three-segment interactions are considered. The present MC data for $A_2$ (along with the previous ones for $\langle S^2\rangle$) may then be consistently explained by the existent theory based on the helical wormlike chain model only if a minor correction is made to the theoretical $A_{2,\Theta}$ in almost the same range where the effects of chain ends are appeciable. The present MC data are also compared with experimental data, and it is shown that the latter may also be similarly explained. © *2003 American Institute of Physics.* [DOI: 10.1063/1.1579682]

## I. INTRODUCTION

In a previous paper,[1] Paper I of this series, possible effects of chain stiffness and chain ends on the mean-square radius of gyration $\langle S^2\rangle$ of a polymer chain have been investigated as a first step of a study of those effects on the intra- and intermolecular excluded-volume effects by Monte Carlo (MC) simulation on the basis of the freely rotating chain[2,3] with a cutoff version[1] of the Lennard-Jones (LJ) 6-12 potential[4] between beads. As was expected, the effects of chain ends on $\langle S^2\rangle$ and therefore on the gyration-radius expansion factor $\alpha_S$ as defined as the square root of the ratio of $\langle S^2\rangle$ to its unperturbed value $\langle S^2\rangle_0$ have been found to be negligibly small. This result is due to the fact that the probability of intramolecular contact is very small because of chain stiffness in the range of small molecular weight $M$ where the effects of chain ends may become appreciable. It has also been shown that the effects of chain stiffness on $\alpha_S$ may be well explained in the quasi-two-parameter (QTP) scheme[2] that all expansion factors, including $\alpha_S$, are functions only of the intramolecular scaled excluded-volume parameter[2,5,6] $\tilde{z}$ instead of the conventional excluded-volume parameter $z$ in the two-parameter (TP) theory.[3]

In this paper, as the next step, we proceed to investigate the effects of chain stiffness and chain ends on the second virial coefficient $A_2$, which is concerned with the intermolecular excluded-volume effect, along the same line as that in Paper I.[1] In contrast to the case of $\alpha_S$ which is a measure of the intramolecular excluded-volume effect, the dependence of $A_2$ on $M$ is remarkably affected, especially for small $M$, by a chemical difference of the chain ends.[2,7,8] In a comparison made so far[2] of experimental values of $A_2$, which necessarily include the effects of chain ends, with its theoretical values without those effects, therefore, they have been removed from the former values by means of the theory[2,7] which takes account of them with some assumptions. Thus the main purpose of the present paper is to examine the validity of this procedure by a comparison of the theory with MC data obtained by varying the ends of the freely rotating chain.

The validity of the above-mentioned procedure of removing the effects of chain ends from observed $A_2$ has been partly confirmed so far by examining the observed dependence on $M$ of $A_2$ at the $\Theta$ temperature, which we denote by $A_{2,\Theta}$. Recall that the $\Theta$ temperature is defined as the temperature at which $A_2$ vanishes for very large $M$ and also $\langle S^2\rangle/M$ becomes there a constant independent of $M$. In the binary cluster approximation,[3] therefore, the theoretical $A_{2,\Theta}$ for a fictitious chain without the effects of chain ends must vanish for all $M$, so that the nonvanishing $A_{2,\Theta}$ arises only from those effects. However, if possible effects of three-segment interactions (ternary cluster integral) are taken into account,[9] $A_{2,\Theta}$ for finite $M$ may in general remain finite even for the fictitious chain, as pointed out by Cherayil *et al.*[10] and by Nakamura *et al.*[11] Further, if this residual contribution is appreciable, the above confirmation based on the assumption that $A_{2,\Theta}=0$ for the fictitious chain requires some reconsideration since it must affect somewhat the estimate of effects of chain ends.[2] Thus the theoretical evaluation of this contribution is also carried out and the result is applied to an analysis of MC data.

The plan of the present paper is as follows: In Sec. II, we give a brief sketch of the simulation model and a numerical recipe for an evaluation of $A_2$. In Sec. IV, we make a rather detailed analysis of MC results for both $\Theta$ and good-solvent

 

systems, which are given in Sec. III, on the basis of the helical wormlike (HW) chain model.[2] First, in Sec. IV A, necessary basic equations for $A_2$ in the HW theory are summerized, and in Sec. IV B, account is taken of possible effects of three-segment interactions within the framework of the first-order perturbation theory, the details of which are given in the Appendix. By the use of the theoretical expressions given in these two sections, then, in Sec. IV C, MC results for the effects of chain ends are analyzed, and finally, in Sec. IV D, the effect of chain stiffness on the behavior of the interpenetration function (without the effects of chain ends) is examined. In Sec. V, we compare the present MC results with some previous and literature experimental data.

## II. MODEL AND METHODS

The MC model used in this study is the same as that used in Paper I,[1] i.e., the freely rotating chain[2,3] composed of $n$ bonds, each of length unity, and of $n+1$ beads, whose centers are located at the $n-1$ junctions of two successive bonds and at the two terminal ends. In what follows, we use the McMillan–Mayer symbolism[3,12] to formulate $A_2$ (two-chain problem), for convenience. Then the $i$th bead ($i=0,1,2,...,n$) of chain $\alpha$ ($\alpha=1,2$) is labeled as $i_\alpha$, and the symbol ($\alpha$) ($\alpha=1,2$) denotes all the coordinates (external and internal) of chain $\alpha$. All the $n-1$ bond angles $\theta$ (not supplements) in each chain are fixed at $\theta=109°$, so that the configuration of chain $\alpha$ may be specified by the set of $n-2$ internal rotation angles $\{\phi_{(n-2)_\alpha}\}=(\phi_{2_\alpha},\phi_{3_\alpha},\ldots,\phi_{(n-1)_\alpha})$ along with the vector position $\mathbf{r}_{\mathrm{c.m.},\alpha}$ of its center of mass and the Euler angles $\Omega_\alpha=(\theta_\alpha,\phi_\alpha,\psi_\alpha)$ representing the orientation of the triangle formed by the first two bonds in an external Cartesian coordinate system, where $\phi_{i_\alpha}$ is the internal rotation angle around the $i$th bond of chain $\alpha$ connecting beads $(i-1)_\alpha$ and $i_\alpha$.

The second virial coefficient $A_2$ may then be expressed in the form[3]

$$A_2=\frac{N_A}{2VM^2}\int F_1(1)F_1(2)\left\{1-\exp\left[-\frac{U_{12}(1,2)}{k_BT}\right]\right\}d(1,2), \tag{1}$$

where $N_A$ is the Avogadro constant, $V$ is the volume of the system, $k_B$ is the Boltzmann constant, $T$ is the absolute temperature, $U_{12}(1,2)$ is the intermolecular potential, and $F_1(\alpha)$ ($\alpha=1,2$) is the one-body (single-chain) distribution function for chain $\alpha$, which is normalized as

$$\frac{1}{V}\int F_1(\alpha)d(\alpha)=1 \quad (\alpha=1,2). \tag{2}$$

The differential volume element $d(1,2)$ for the two chains in Eq. (1) is defined by

$$d(1,2)=d(1)d(2), \tag{3}$$

and the one $d(\alpha)$ for chain $\alpha$ in Eqs. (2) and (3) may be explicitly written as

$$d(\alpha)=\sin^{n-1}\theta\, d\mathbf{r}_{\mathrm{c.m.},\alpha}\, d\Omega_\alpha\, d\{\phi_{(n-2)_\alpha}\} \quad (\alpha=1,2) \tag{4}$$

with $d\Omega_\alpha=\sin\theta_\alpha\, d\theta_\alpha\, d\phi_\alpha\, d\psi_\alpha$. As schematically depicted in Fig. 1 (compare with Fig. 1 of Ref. 1 and Fig. 2 of Ref. 7),

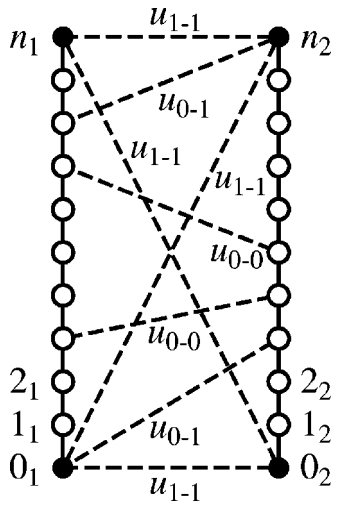


FIG. 1. Three kinds of intermolecular interactions (contacts) between beads.

$U_{12}(1,2)$ in Eq. (1) is assumed to be composed of three kinds of intermolecular interactions between beads as

$$\begin{aligned}U_{12}(1,2)=&\sum_{i_1=1}^{n-1}\sum_{i_2=1}^{n-1}u_{0\text{-}0}(R_{i_1i_2})+\sum_{i_1=1}^{n-1}[u_{0\text{-}1}(R_{i_1 0_2})\\&+u_{0\text{-}1}(R_{i_1 n_2})]+\sum_{i_2=1}^{n-1}[u_{0\text{-}1}(R_{0_1 i_2})\\&+u_{0\text{-}1}(R_{n_1 i_2})]+u_{1\text{-}1}(R_{0_1 0_2})+u_{1\text{-}1}(R_{0_1 n_2})\\&+u_{1\text{-}1}(R_{n_1 0_2})+u_{1\text{-}1}(R_{n_1 n_2}),\end{aligned} \tag{5}$$

where $u_{1-1}$, $u_{0-1}$, and $u_{0-0}$ are the pair potentials (of mean force) between the end beads, between one end and intermediate beads, and between intermediate beads, respectively. The summation (or dummy) index $i_\alpha$ ($\alpha=1,2$) in Eq. (5) indicates the $i_\alpha$th ($i_\alpha=1,2,\ldots,n-1$) intermediate bead of chain $\alpha$, and the indices $0_\alpha$ and $n_\alpha$ the two end beads of chain $\alpha$. Further, $R_{i_1i_2}$ represents the distance between the centers of the $i_1$th intermediate bead of chain 1 and the $i_2$th one of chain 2, $R_{i_1 0_2}$ the distance between the centers of the $i_1$th intermediate bead of chain 1 and bead $0_2$, and so on. We note that the pairwise decomposability of the intermolecular potential energy $U_{12}$ has been assumed, as done in the single-chain problem in Paper I.[1]

We use as the pair potential $u_{\xi-\eta}(R)$ ($\xi,\eta=0,1$) in Eq. (5) the same one as that introduced in Paper I,[1] i.e., the LJ 6-12 potential with the collision diameter $\sigma_{\xi-\eta}$, the depth $\epsilon_{\xi-\eta}$ of the potential well at its minimum, and its attractive tail truncated at $R=3\sigma_{\xi-\eta}$. Among the six parameters $\sigma_{0-0}$, $\sigma_{0-1}$, $\sigma_{1-1}$, $\epsilon_{0-0}$, $\epsilon_{0-1}$, and $\epsilon_{1-1}$ characterizing the interactions between beads, $\sigma_{0-1}$ and $\epsilon_{0-1}$ have been subordinated to the others by the use of the Lorentz and Berthelot combining rules,[4] respectively; i.e., $\sigma_{0-1}$ is the arithmetic mean $(\sigma_{0-0}+\sigma_{1-1})/2$ of $\sigma_{0-0}$ and $\sigma_{1-1}$, and $\epsilon_{0-1}$ is the geometric mean $(\epsilon_{0-0}\epsilon_{1-1})^{1/2}$ of $\epsilon_{0-0}$ and $\epsilon_{1-1}$. Further, $\sigma_{0-0}$ and $\sigma_{1-1}$ have been set equal to unity, so that $\sigma_{0-1}=1$ (touched-bead model), for simplicity. Thus the parameters have been reduced to $\epsilon_{0-0}$ and $\epsilon_{1-1}$. In what follows,

the reduced temperatures $T^*_{\xi-\xi}\equiv k_BT/\epsilon_{\xi-\xi}$ ($\xi=0,1$) are used instead of $\epsilon_{\xi-\xi}$ themselves as in Paper I.[1] Note that $T^*_{0-1}=(T^*_{0-0}T^*_{1-1})^{1/2}$.

Now the procedure of evaluating numerically $A_2$ given by Eq. (1) is in principle the same as those used in other MC studies of $A_2$.[13–15] Equation (1) may be rewritten in the form

$$A_2=\frac{2\pi N_A}{M^2}\int_0^\infty\left\{1-\exp\left[-\frac{\overline{U}_{12}(r)}{k_BT}\right]\right\}r^2\,dr, \tag{6}$$

where $\overline{U}_{12}(r)$ is the averaged intermolecular potential as a function of the distance $r=|\mathbf{r}|$ between the centers of mass of the two chains (with $\mathbf{r}=\mathbf{r}_{\mathrm{c.m.},2}-\mathbf{r}_{\mathrm{c.m.},1}$) defined by

$$\overline{U}_{12}(r)=-k_BT\ln\left\langle\exp\left[-\frac{U_{12}(1,2)}{k_BT}\right]\right\rangle_r \tag{7}$$

with $\langle\cdots\rangle_r$ indicating the conditional average formally defined by

$$\langle\cdots\rangle_r=\frac{1}{V}\int F_1(1)F_1(2)\cdots d(1,2)/d\mathbf{r}. \tag{8}$$

This is the equilibrium average taken over the configurations of the two chains with $\mathbf{r}$ fixed by the use of the single-chain distribution function $F_1(\alpha)$ for each with the intramolecular excluded-volume effect (see Fig. 1 of Ref. 1). This average may be calculated by the use of a set of chain (sample) configurations generated properly by MC simulation, as follows. First, a set of $N_s$ sample configurations are generated by a MC run following the procedure described in Paper I.[1] Next we randomly sample a pair of chain configurations from the set (of size $N_s$) and calculate the intermolecular potential $U_{12}(1,2)/k_BT$ from Eq. (5) at given $r$ after randomizing the orientations of the two configurations in the external coordinate system. Finally, we adopt as the value of $\exp[-\overline{U}_{12}(r)/k_BT]$ a mean of values of $\exp[-U_{12}(1,2)/k_BT]$ so obtained for $N_p$ sample pairs (of chain configurations). With the values of $\exp[-\overline{U}_{12}(r)/k_BT]$ so obtained for various values of $r$, the quantity $A_2M^2$ for given $n$ and at given $T^*_{0-0}$ and $T^*_{1-1}$ may then be calculated from Eq. (6) by numerical integration with the use of the trapezoidal rule formula. In the practical evaluation of $\overline{U}_{12}$ (and $A_2$), several sets of $10^5$ ($=N_s$) sample configurations have been generated by MC runs, and $10^6$ or $10^7$ ($=N_p$) sample pairs have been taken from each set. Then the total number of sample pairs is equal to the number $N_p$ of sample pairs in each MC run multiplied by the number of MC runs. Further, we have changed integration variables from $r$ to a reduced one, for convenience (see the next section).

In computing $U_{12}(1,2)/k_BT$ for each pair of sample configurations (chains), we have used the following algorithm for a speedy calculation of the double sum in Eq. (5). We locate the center of mass of one of the two chains at the origin of the external coordinate system $(x, y, z)$ and that of the other at $(0, 0, r)$. First, we prepare a list of those pairs of intermediate beads of different chains for which the distance between their centers can become smaller than or equal to $3\sigma_{0-0}$ when $r$ varies. It may be done by listing those pairs of beads for which the distance between the projections of their centers onto the $xy$ plane is smaller than or equal to $3\sigma_{0-0}$. Then we sum up the pair potentials $u_{0-0}$ only of those pairs for various values of $r$. We note that the "zippering" method[16,17] has been used in the above examination in the $xy$ plane.

All the numerical work has been done by the use of a personal computer with an AMD Athlon XP 2200+ CPU. A source program coded in C has been compiled by the GNU C compiler version 2.95.4 with real variables of double precision. In the program, the subroutine package MT19937 supplied by Matsumoto and Nishimura[18] has been used instead of the subroutine RAND included in the standard C library.

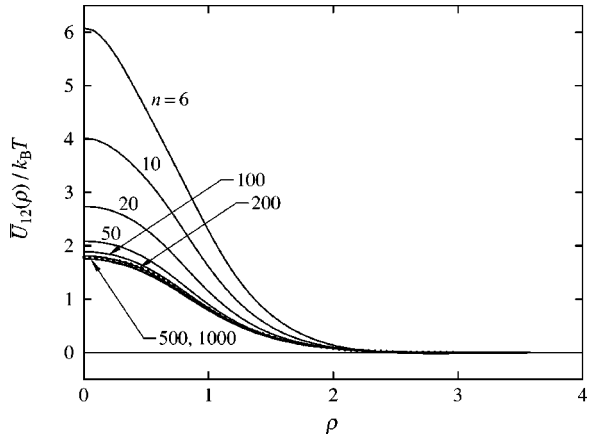


FIG. 2. Plots of $\overline{U}_{12}(\rho)/k_BT$ against $\rho$ at $T^*_{0-0}=T^*_{1-1}=8.0$ for the MC chains with the indicated values of $n$. The dotted curve represents the values obtained by Bolhuis *et al.* (Ref. 15) for the self-avoiding-walk chain of 8000 steps on a simple-cubic lattice.

## III. RESULTS

### A. Averaged intermolecular potential

Equation (6) may be rewritten in the form

$$A_2=4\pi^{3/2}N_A\frac{\langle S^2\rangle^{3/2}}{M^2}\Psi_{\mathrm{ap}}, \tag{9}$$

where the dimensionless quantity $\Psi_{\mathrm{ap}}$ is the *apparent* interpenetration function[8] defined as above from the whole $A_2$ including the effects of chain ends, and therefore is also defined by

$$\Psi_{\mathrm{ap}}=\frac{1}{2\pi^{1/2}}\int_0^\infty\left\{1-\exp\left[-\frac{\overline{U}_{12}(\rho)}{k_BT}\right]\right\}\rho^2\,d\rho \tag{10}$$

with $\rho=r/\langle S^2\rangle^{1/2}$ the reduced distance between the centers of mass of two chains. It is seen from these equations that the behavior of $A_2$ is closely related not only to that of $\langle S^2\rangle$ but also to that of the averaged intermolecular potential $\overline{U}_{12}$. First, in this section, therefore we give MC results for the latter to examine its behavior.

Figure 2 shows plots of $\overline{U}_{12}(\rho)/k_BT$ against $\rho$ at reduced temperatures $T^*_{0-0}=T^*_{1-1}=8.0$. We note that the condition $T^*_{0-0}=8.0$ corresponds to a good-solvent system.[1] The solid line segments connect the present MC values for the indicated values of $n$. The total numbers of sample pairs for the

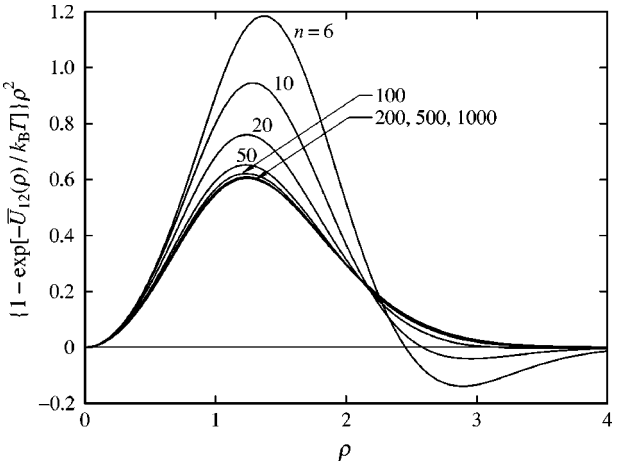


FIG. 3. Plots of $\{1-\exp[-\overline{U}_{12}(\rho)/k_BT]\}\rho^2$ against $\rho$ at $T^*_{0-0}=T^*_{1-1}=8.0$ for the indicated values of $n$.

evaluation of $\overline{U}_{12}$ are $10^7$ for $n=6-100$, $3\times10^6$ for $n=200$ and 500, and $2\times10^6$ for $n=1000$. It is seen that $\overline{U}_{12}(\rho)/k_BT$ as a function of $n$ in the range of $\rho\lesssim2$ decreases monotonically with increasing $n$ and approaches a constant in the limit of $n\to\infty$ at all $\rho$. For comparison, the values obtained by Bolhuis *et al.*[15] for the self-avoiding-walk chain of 8000 steps on a simple-cubic lattice are also shown in Fig. 2 by the dotted curve, which is seen to be close to the solid curve for $n=500$ or 1000. This agreement is consistent with the common notion that $\overline{U}_{12}(\rho)$ for good-solvent systems converges to a universal function independent of chain model in the limit of $n\to\infty$.

Values of $\{1-\exp[-\overline{U}_{12}(\rho)/k_BT]\}\rho^2$ are plotted against $\rho$ in Fig. 3 with the same present MC data as those in Fig. 1. The solid line segments connect the present MC values for the indicated values of $n$. It is interesting to note that the attractive tails exist and contribute to $A_2$ for $n=6$ and 10, although they are not clearly seen in Fig. 2.

Figure 4 shows plots of $\{1-\exp[-\overline{U}_{12}(\rho)/k_BT]\}\rho^2$ against $\rho$ at reduced temperatures $T^*_{0-0}=T^*_{1-1}=3.72$. We

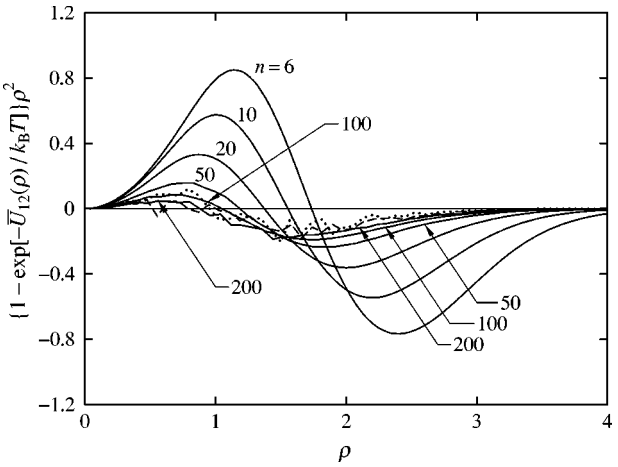


FIG. 4. Plots of $\{1-\exp[-\overline{U}_{12}(\rho)/k_BT]\}\rho^2$ against $\rho$ at $T^*_{0-0}=T^*_{1-1}=3.72$ ($\Theta^*$) for the indicated values of $n$. The dashed and dotted line segments connect the values for $n=500$ and 1000, respectively.

TABLE I. Values of $\Psi_{ap}$ at $T^*_{0-0}=8.0$.

| $n$ | $\Psi_{ap}$ (error) | $N_p$ | Number of MC runs |
|---|---|---|---|
| | $T^*_{1-1}=3.72$ | | |
| 6 | $0.264_1$ (0.0006) | $10^6$ | 10 |
| 10 | $0.262_1$ (0.0005) | $10^6$ | 10 |
| 20 | $0.253_7$ (0.0003) | $10^6$ | 10 |
| 50 | $0.245_7$ (0.0005) | $10^6$ | 10 |
| 100 | $0.242_3$ (0.0003) | $10^6$ | 10 |
| 200 | $0.241_2$ (0.0002) | $10^6$ | 3 |
| | $T^*_{1-1}=8.0$ | | |
| 6 | $0.362_2$ (0.0006) | $10^6$ | 10 |
| 10 | $0.315_4$ (0.0004) | $10^6$ | 10 |
| 20 | $0.266_7$ (0.0004) | $10^6$ | 10 |
| 50 | $0.253_9$ (0.0003) | $10^6$ | 10 |
| 100 | $0.246_8$ (0.0003) | $10^6$ | 10 |
| 200 | $0.243_2$ (0.0003) | $10^6$ | 3 |
| 500 | $0.242_6$ (0.0000) | $10^6$ | 3 |
| 1000 | $0.243_0$ (0.0002) | $10^6$ | 2 |
| | $T^*_{1-1}=20.0$ | | |
| 6 | $0.414_4$ (0.0003) | $10^6$ | 10 |
| 10 | $0.345_5$ (0.0005) | $10^6$ | 10 |
| 20 | $0.292_2$ (0.0004) | $10^6$ | 10 |
| 50 | $0.259_8$ (0.0005) | $10^6$ | 10 |
| 100 | $0.248_9$ (0.0003) | $10^6$ | 10 |
| 200 | $0.244_4$ (0.0002) | $10^6$ | 3 |

note that the condition $T^*_{0-0}=3.72$ corresponds to the $\Theta$ temperature at which $\langle S^2\rangle/n$ becomes a constant independent of $n$ in the limit of $n\to\infty$,[1] so that we set $\Theta^*=3.72$. The solid line segments connect the present MC values for the indicated values of $n$, and the dashed and dotted line segments connect those for $n=500$ and 1000, respectively. The total numbers of sample pairs for the evaluation of $\overline{U}_{12}$ are $10^7$ for $n=6-50$, $10^8$ for $n=100$ and 200, and $5\times10^7$ for $n=500$ and 1000. Statistical errors in the MC values for $n=500$ and 1000 are appreciable. In contrast to the picture in the binary cluster approximation, in which $1-\exp[-\overline{U}_{12}(\rho)/k_BT]$ vanishes at $\Theta$, there are observed a repulsive core and an attractive tail in $\{1-\exp[-\overline{U}_{12}(\rho)/k_BT]\}\rho^2$ over the whole range of $n$ examined. We note that the corresponding behavior of $\overline{U}_{12}$ or its functions at $\Theta$ has been observed in previous MC studies based on other models.[13,14,19] Although it is difficult to conjecture the asymptotic shape of the plot in the limit of $n\to\infty$ only from the present MC data shown in Fig. 4, it may be considered that $\{1-\exp[-\overline{U}_{12}(\rho)/k_BT]\}\rho^2$ at $\Theta$ converges to a limiting function having nonzero values, as discussed in Sec. IV B.

### B. Second virial coefficient

Now we give results for $A_2$. The values of $\Psi_{ap}$ calculated from Eq. (10) by numerical integration of the function $\{1-\exp[-\overline{U}_{12}(\rho)/k_BT]\}\rho^2$ shown in Figs. 3 and 4 for the cases of $T^*_{0-0}=8.0$ (good-solvent condition) and 3.72 ($\Theta$ condition) are given in Tables I and II, respectively, thus the values in the latter giving $A_{2,\Theta}$. In the third and fourth columns in each table are also given the values of the number $N_p$ of sample pairs (of chain configurations) taken from the set of $10^5$ ($=N_s$) sample configurations in a MC run and

TABLE II. Values of $\Psi_{ap}$ at $T^*_{0-0}=3.72$ ($\Theta^*$).

| $n$ | $\Psi_{ap}$ (error) | $N_p$ | Number of MC runs |
|---|---|---|---|
| | $T^*_{1-1}=3.72$ | | |
| 6 | $-0.049_2(0.0006)$ | $10^6$ | 10 |
| 10 | $-0.050_4(0.0007)$ | $10^6$ | 10 |
| 20 | $-0.049_7(0.0006)$ | $10^6$ | 10 |
| 50 | $-0.049_3(0.0012)$ | $10^6$ | 10 |
| 100 | $-0.050_9(0.0014)$ | $10^7$ | 10 |
| 200 | $-0.054_1(0.0026)$ | $10^7$ | 10 |
| 500 | $-0.040_4(0.0062)$ | $10^7$ | 5 |
| 1000 | $-0.025_5(0.0158)$ | $10^7$ | 5 |
| | $T^*_{1-1}=8.0$ | | |
| 6 | $0.115_4(0.0005)$ | $10^6$ | 10 |
| 10 | $0.056_8(0.0005)$ | $10^6$ | 10 |
| 20 | $0.012_5(0.0009)$ | $10^6$ | 10 |
| 50 | $-0.017_2(0.0006)$ | $10^6$ | 10 |
| 100 | $-0.031_5(0.0021)$ | $10^6$ | 10 |
| 200 | $-0.036_7(0.0063)$ | $10^6$ | 10 |
| 500 | $-0.029_5(0.0109)$ | $10^6$ | 5 |
| | $T^*_{1-1}=20.0$ | | |
| 6 | $0.207_5(0.0004)$ | $10^6$ | 10 |
| 10 | $0.118_7(0.0005)$ | $10^6$ | 10 |
| 20 | $0.050_1(0.0006)$ | $10^6$ | 10 |
| 50 | $0.002_9(0.0010)$ | $10^6$ | 10 |
| 100 | $-0.016_7(0.0017)$ | $10^6$ | 10 |
| 200 | $-0.032_8(0.0082)$ | $10^6$ | 10 |
| 500 | $-0.021_1(0.0125)$ | $10^6$ | 5 |

those of the number of MC runs carried out to evaluate $\Psi_{ap}$, respectively. Specifically, for example, for the chain with $n=6$ at $T^*_{0-0}=8.0$ and $T^*_{1-1}=3.72$ in Table I, 10 sets of $10^5$ sample configurations have been generated by 10 independent MC runs, and $\Psi_{ap}$ has been evaluated by the use of $10^6$ sample pairs taken from each set. Then the final results for $\Psi_{ap}$ and its statistical errors, which are given in the second column of each table, have been obtained as the mean and the standard deviation of the 10 values of $\Psi_{ap}$ so evaluated, respectively. Thus $10^7$ sample pairs in total have been used to determine the value of $\Psi_{ap}$ in this case. It is seen from Table II that the statistical errors for the chains with $n=500$ and 1000 at $T^*_{0-0}=3.72$ ($\Theta^*$) are appreciably large, as is natural from the results in Fig. 4.

In the other MC studies[13–15] of $A_2$ mentioned in Sec. II, MC data for $A_2$ have been given in certain reduced units, so that it is difficult to compare absolutely those with experimental data. In order to compare the present MC data for $A_2$ with experimental ones, therefore, we evaluate the former in real units. For this purpose, we rewrite Eq. (9) as

$$A_2=4\pi^{3/2}N_A\frac{l^3(\langle S^2\rangle_{l=1}/n)^{3/2}}{M_b^2 n^{1/2}}\Psi_{ap}, \tag{11}$$

where $l$ is the real bond length, which, for convenience, has been chosen to be unity in the present and previous[1] MC studies, $\langle S^2\rangle_{l=1}$ is the MC value of $\langle S^2\rangle$ evaluated with $l=1$, and $M_b$ is the molecular weight per bond. The MC values of $A_2$ in real units may then be calculated from Eq. (11) with the MC values of $\Psi_{ap}$ (given in Tables I and II) and $\langle S^2\rangle_{l=1}/n$ if the values of $l$ and $M_b$ in real units are properly chosen. It is well known that the equilibrium conformational

TABLE III. Values of $\langle S^2\rangle_{l=1}/n$ at $T^*_{0-0}=8.0$.

| $n$ | $\langle S^2\rangle_{l=1}/n$ (error %) | Acceptance fraction | Number of MC runs |
|---|---|---|---|
| | $T^*_{1-1}=3.72$ | | |
| 6 | $0.288_0$ (0.0) | 9/10 | 10 |
| 10 | $0.314_1$ (0.1) | 17/20 | 10 |
| 20 | $0.358_5$ (0.1) | 33/40 | 10 |
| 50 | $0.427_2$ (0.1) | 75/100 | 10 |
| 100 | $0.486_1$ (0.1) | 140/200 | 10 |
| 200 | $0.550_3$ (0.1) | 324/500 | 10 |
| | $T^*_{1-1}=8.0$ | | |
| 6 | $0.289_2$ (0.1) | 9/10 | 10 |
| 10 | $0.315_8$ (0.1) | 18/20 | 10 |
| 20 | $0.369_9$ (0.1) | 33/40 | 10 |
| | $T^*_{1-1}=20.0$ | | |
| 6 | $0.289_6$ (0.0) | 9/10 | 10 |
| 10 | $0.316_8$ (0.1) | 18/20 | 10 |
| 20 | $0.360_9$ (0.1) | 33/40 | 10 |
| 50 | $0.429_1$ (0.1) | 76/100 | 10 |
| 100 | $0.487_3$ (0.2) | 141/200 | 10 |
| 200 | $0.551_2$ (0.1) | 325/500 | 10 |

behavior of the freely rotating chain may be well represented by the Kratky–Porod (KP) wormlike chain,[2,20] and in fact, the MC data for $\langle S^2\rangle_{l=1}/n$ at $\Theta^*$ have been analyzed in Paper I[1] to determine the reduced stiffness parameter $\lambda^{-1}/l=3.0_1$ and the number $ln_L=1.2_4$ of bonds per unit reduced contour length (both in units of the bond length), assuming the KP chain. With values of the stiffness parameter $\lambda^{-1}$ and the shift factor $M_L$ as defined as the molecular weight per unit contour length determined for a KP-type real polymer chain, we may therefore assign values to $l$ and also $M_b$ by the use of the relation,

$$M_L=n_L M_b. \tag{12}$$

We adopt the respective values 16.8 Å and 35.8 $Å^{-1}$ of $\lambda^{-1}$ and $M_L$ determined from an analysis of previous data for $\langle S^2\rangle$ of atactic polystyrene ($a$-PS) in cyclohexane at 34.5 °C ($\Theta$)[21,22] to obtain $l=5.5_8$ Å and $M_b=1.6_1\times10^2$, the details of the analysis (as the KP chain) being omitted. We note that strictly, the data for $a$-PS should be analyzed on the basis of the HW chain model.[2]

The values of $\langle S^2\rangle_{l=1}/n$ at $T^*_{0-0}=8.0$ and $T^*_{0-0}=3.72$ required for the evaluation of $A_2$ are given in Tables III and IV, respectively, along with the values of the acceptance fraction[1] and those of the number of MC runs. In addition to them, the values given in Tables I and II of Paper I[1] are also used in what follows.

Figure 5 shows double-logarithmic plots of $A_2$ (in $cm^3$ mol/$g^2$) against $M$ ($=nM_b$) at $T^*_{0-0}=8.0$ (good-solvent system). The open circles, each with center dot, represent the values calculated from Eq. (11) with the values of $\Psi_{ap}$ given in Table I and those of $\langle S^2\rangle_{l=1}/n$ given in Table III and Table I of Paper I,[1] and also with the above-estimated values of $l$ and $M_b$ at $T^*_{1-1}=20.0$ (pip up), 8.0 (pip right), and 3.72 (pip down). The solid curve connects smoothly the data points at each $T^*_{1-1}$. It is seen that $A_2$ increases with increasing $T^*_{1-1}$ for $M\lesssim3\times10^4$ because of the effects of chain ends.

TABLE IV. Values of $\langle S^2\rangle_{l=1}/n$ at $T^*_{0-0}=3.72$ ($\Theta^*$).

| $n$ | $\langle S^2\rangle_{l=1}/n$ (error %) | Acceptance fraction | Number of MC runs |
|---|---|---|---|
| | $T^*_{1-1}=3.72$ | | |
| 6 | $0.285_7$ (0.1) | 9/10 | 10 |
| | $T^*_{1-1}=8.0$ | | |
| 6 | $0.287_6$ (0.0) | 9/10 | 10 |
| 200 | $0.392_9$ (0.1) | 221/500 | 10 |
| 500 | $0.401_2$ (0.2) | 333/1000 | 5 |
| | $T^*_{1-1}=20.0$ | | |
| 6 | $0.288_8$ (0.0) | 9/10 | 10 |
| 10 | $0.309_8$ (0.1) | 17/20 | 10 |
| 20 | $0.337_6$ (0.1) | 31/40 | 10 |
| 50 | $0.367_4$ (0.2) | 64/100 | 10 |
| 100 | $0.383_2$ (0.1) | 108/200 | 10 |
| 200 | $0.394_1$ (0.2) | 222/500 | 10 |
| 500 | $0.400_5$ (0.2) | 334/1000 | 5 |

Figure 6 shows plots of $A_{2,\Theta}$ against the logarithm of $M$ at $T^*_{0-0}=3.72$ ($\Theta^*$). The open circles represent the values calculated from Eq. (11) with the values of $\Psi_{ap}$ given in Table II and those of $\langle S^2\rangle_{l=1}/n$ given in Table IV and Tables I and II of Paper I,[1] and also with the above-estimated values of $l$ and $M_b$ at $T^*_{1-1}=20.0$ (pip up), 8.0 (pip right), and 3.72 (pip down). The solid curve represents the theoretical values at each $T^*_{1-1}$, and the dashed curve those for the fictitious chain without the effects of chain ends but with three-segment interactions. These theoretical values are obtained and discussed in Secs. IV C and IV B, respectively. As in the case of $T^*_{0-0}=8.0$ shown in Fig. 5, the effects of chain ends become appreciable for $M\lesssim 3\times 10^4$, and $A_2$ increases there with increasing $T^*_{1-1}$. It is seen that $A_{2,\Theta}$ (at $\Theta^*$) first decreases from zero and then increases with decreasing $M$. We note that this decrease in $A_{2,\Theta}$ corresponds to the result by Bruns[23] for lattice chains that the depth of an attractive well for which $A_2$ vanishes increases with increasing $n$ (or $M$).

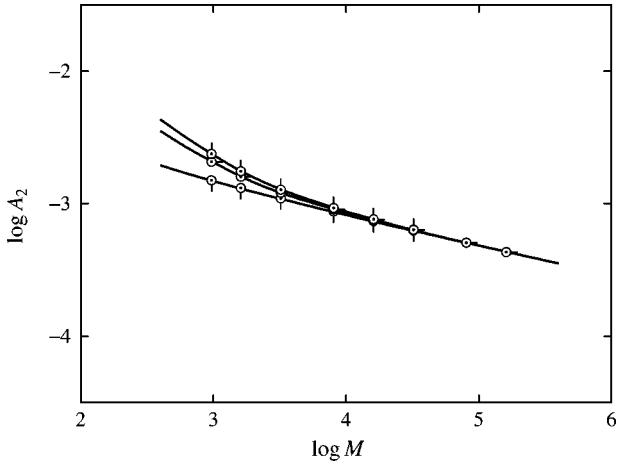


FIG. 5. Double-logarithmic plots of $A_2$ (in cm$^3$ mol/g$^2$) against $M$ at $T^*_{0-0}=8.0$. The open circles, each with center dot, represent the values at $T^*_{1-1}=20.0$ (pip up), 8.0 (pip right), and 3.72 (pip down), the solid curve connecting smoothly the data points at each $T^*_{1-1}$.

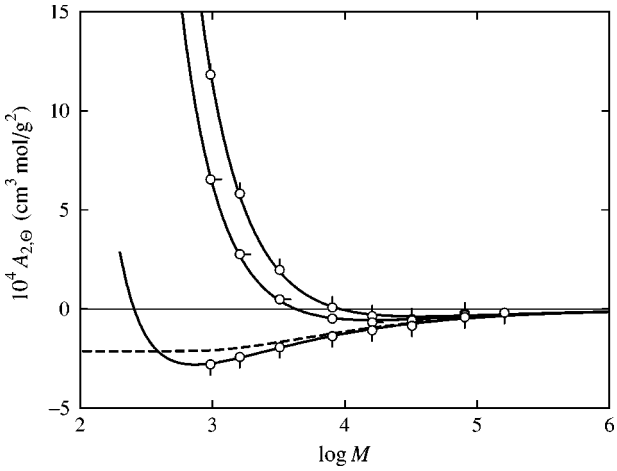


FIG. 6. Plots of $A_{2,\Theta}$ against $\log M$ at $T^*_{0-0}=3.72$ ($\Theta^*$). The open circles represent the values at $T^*_{1-1}=20.0$ (pip up), 8.0 (pip right), and 3.72 (pip down). The solid curves represent the theoretical values of $A_{2,\Theta}$ ($=A^{(HW)}_{2,\Theta}+A^{(E)}_2$) at $T^*_{1-1}=20.0$, 8.0, and 3.72 from top to bottom, and the dashed curve those of $A^{(HW)}_{2,\Theta}$ (see the text).

## IV. ANALYSIS AND DISCUSSION

### A. Basic equations

In this section, we summarize basic equations in the HW theory[2,7,24] necessary for an analysis of the MC data for $A_2$ given in Sec. III. It takes account of both effects of chain stiffness and chain ends on the basis of the HW bead model (with excluded volume), where excluded-volume interactions are considered in the binary cluster approximation,[3] and simply those for the latter effects in the single-contact approximation.[3] (Note that the latter approximation is good enough to consider them for small $M$.) The model is such that $n+1$ beads are arrayed with spacing $a$ between them along the contour of total length $L=na$, where the $n-1$ intermediate beads are identical and the two end beads are different from the intermediate ones and also in general from each other in species. Identical excluded-volume interactions between intermediate beads are expressed in terms of the conventional binary-cluster integral, which we here denote by $\beta_2$, while two kinds of effective excess binary-cluster integrals $\beta_{2,1}$ and $\beta_{2,2}$ are necessary in order to express interactions between unlike (and like end) beads, $\beta_{2,1}$ being associated with one end bead and $\beta_{2,2}$ with two end ones. The HW model itself[2] is defined in terms of three basic model parameters: the constant differential-geometrical curvature $\kappa_0$ and torsion $\tau_0$ of its characteristic helix taken at the minimum zero of its elastic energy and the stiffness parameter $\lambda^{-1}$.

According to the theory,[2,7] $A_2$ may be written in the form

$$A_2=A_2^{(HW)}+A_2^{(E)}, \tag{13}$$

where $A_2^{(HW)}$ is the part of $A_2$ without the effects of chain ends, or $A_2$ for the fictitious chain composed of $n+1$ identical beads, and $A_2^{(E)}$ represents the contribution of the effects of chain ends to $A_2$. The first term $A_2^{(HW)}$ may be given by

$$A_2^{(HW)}=(N_A c_\infty^{3/2}L^2B/2M^2)h(\hat{z}), \tag{14}$$

where the constant $c_\infty$ and the excluded-volume strength $B$ are defined by

$$c_\infty = \frac{4+(\lambda^{-1}\tau_0)^2}{4+(\lambda^{-1}\kappa_0)^2+(\lambda^{-1}\tau_0)^2} \tag{15}$$

and

$$B = \beta_2/a^2 c_\infty^{3/2}, \tag{16}$$

respectively. The so-called $h$ function in Eq. (14) is given by

$$h(\hat{z}) = (1+7.74\hat{z}+52.3\hat{z}^{27/10})^{-10/27} \tag{17}$$

with

$$\hat{z} = \tilde{z}/\alpha_S^3. \tag{18}$$

In Eq. (18), $\tilde{z}$ is the intermolecular scaled excluded-volume parameter defined by

$$\tilde{z} = [Q(\lambda L)/2.865]z, \tag{19}$$

where the coefficient $Q(L)$ as a function of (reduced) $L$ represents the effects of chain stiffness on the intermolecular excluded-volume effect, as explicitly given below, and the conventional excluded-volume parameter[3] $z$ is now redefined by

$$z = (3/2\pi)^{3/2}(\lambda B)(\lambda L)^{1/2}. \tag{20}$$

According to the QTP scheme or the Yamakawa–Stockmayer–Shimada (YSS) theory,[2,5,6,24] the gyration-radius expansion factor $\alpha_S$ in Eq. (18) may be given by the Domb–Barrett equation,[25]

$$\alpha_S^2 = [1+10\tilde{z}+(70\pi/9+10/3)\tilde{z}^2+8\pi^{3/2}\tilde{z}^3]^{2/15} \times [0.933+0.067\exp(-0.85\tilde{z}-1.39\tilde{z}^2)] \tag{21}$$

with the intramolecular scaled excluded-volume parameter $\tilde{z}$ defined by

$$\tilde{z} = (3/4)K(\lambda L)z \tag{22}$$

in place of $z$. In Eq. (22), the coefficient $K(L)$ as a function of (reduced) $L$ represents the effects of chain stiffness on the intramolecular excluded-volume effect and is given by

$$\begin{aligned} K(L) &= \tfrac{4}{3}-2.711L^{-1/2}+\tfrac{7}{6}L^{-1} \quad \text{for } L>6 \\ &= L^{-1/2}\exp(-6.611L^{-1}+0.9198 \\ &\quad +0.035\,16L) \quad \text{for } L\leqslant 6. \end{aligned} \tag{23}$$

We note that $K(L)$ approaches the coil-limiting value 4/3 of the coefficient of $z$ in the first-order perturbation theory[3] of the mean-square end-to-end distance $\langle R^2\rangle$ for the random-flight chain in the limit of $L\to\infty$ and vanishes extremely rapidly at small $L$, for which there are no intramolecular contacts between beads.

The coefficient $Q(L)$ in Eq. (19) is given for $L\gtrsim 1$ in a very good approximation by[2,7]

$$\begin{aligned} Q(L) = &-\frac{128\sqrt{2}}{15}-2.531L^{-1/2}-2.586L^{-1}+1.985L^{-3/2} \\ &-1.984L^{-2}-0.9292L^{-5/2}+0.1223L^{-3}+\tfrac{8}{5}x^{5/2} \\ &+\tfrac{2}{3}x^{3/2}(8+\tfrac{1}{6}L^{-1})+x^{1/2}(8-13.53L^{-1} \\ &+0.2804L^{-2})-x^{-1/2}L^{-1}(0.3333-5.724L^{-1} \\ &+0.7974L^{-2})-x^{-3/2}L^{-2}(0.3398-0.7146L^{-1}) \end{aligned} \tag{24}$$

with

$$x = 1+0.961L^{-1}. \tag{25}$$

We simply put $h=1$ (rod limit) for $L\lesssim 1$, in which range Eq. (24) is not valid. We note that $Q(L)$ increases monotonically with increasing $L$ and approaches the coil-limiting value 2.865 of the (negative) coefficient of $z$ in the first-order perturbation theory[3] of the $h$ function for the random-flight chain in the limit of $L\to\infty$. We also note that $L$ is related to $M$ by the equation

$$L = M/M_L. \tag{26}$$

The second term $A_2^{(E)}$ on the right-hand side of Eq. (13) may be written in the form,[2,7]

$$A_2^{(E)} = a_1 M^{-1}+a_2 M^{-2}, \tag{27}$$

where

$$\begin{aligned} a_1 &= 2N_A\beta_{2,1}/M_0, \\ a_2 &= 2N_A\Delta\beta_{2,2} \end{aligned} \tag{28}$$

with $M_0$ the molecular weight of the bead and with

$$\Delta\beta_{2,2} = \beta_{2,2}-2\beta_{2,1}. \tag{29}$$

Within the framework of the above binary-cluster theory, the first term $A_2^{(\mathrm{HW})}$ on the right-hand side of Eq. (13) vanishes at the $\Theta$ temperature, at which $\beta_2=0$, so that a possible deviation of $A_{2,\Theta}$ from zero must then arise only from the second term $A_2^{(E)}$.

### B. Effects of three-segment interactions

As shown in Fig. 6 of Sec. III B, the present MC values of $A_{2,\Theta}$ at $T^*_{0-0}=3.72$ ($\Theta^*$) remain slightly negative even in the range of $M\gtrsim 3\times 10^4$, in which the effects of chain ends are very small, i.e., $A_2^{(E)}\simeq 0$. Such behavior of $A_{2,\Theta}$ cannot be explained within the framework of the binary cluster theory summarized in the last section. As mentioned in Sec. I, this deviation may be regarded as arising from the residual contribution of three-segment interactions. In fact, Nakamura *et al.*[11] have evaluated this contribution as a higher-order term involved in the first-order perturbation theory developed long before[9] for the random-flight chain with three-segment interactions, and showed that the downward deviation of $A_{2,\Theta}$ from zero is proportional to $M^{-1/2}$. In this section, we pursue further this problem along the same line on the basis of the HW chain instead of the random-flight chain. Although there have been some arguments[10,26] about

the behavior of polymer chains near the Θ temperature in relation to the tricritical point,[26] they are beyond the scope of the present problem.

For convenience, we begin by presenting the results of the first-order perturbation theory of $A_2$ and also the end-distance expansion factor $\alpha_R$ as defined as the square root of the ratio of $\langle R^2\rangle$ to its unperturbed value $\langle R^2\rangle_0$ for the random-flight chain, the latter result being a new one. If we retain terms of $A_2$ proportional to $n^{-1/2}\beta_2$ and $n^{-1/2}\beta_3$ with $\beta_3$ the ternary cluster integral in addition to those proportional to $\beta_2$ and $\beta_3$, following the procedure in the perturbation theory with consideration of $\beta_3$,[9] then $A_2$ may be given by[11]

$$A_2=\frac{N_A n^2}{2M^2}\left[\beta-8\left(\frac{3}{2\pi a^2}\right)^{3/2}\beta_3 n^{-1/2}+\cdots\right] \tag{30}$$

with $\beta$ the *effective* binary-cluster integral defined by

$$\beta=\beta_2+4\left(\frac{3}{2\pi a^2}\right)^{3/2}\beta_3. \tag{31}$$

Recall that for the smoothed-density model, the effective $\beta$ depends on $n$, the result being inconsistent with experiment.[2,9] The parameter $a$ in Eqs. (30) and (31) denotes the effective bond length of the random-flight chain (not the spacing between beads in the HW bead model) as far as the theoretical results for the random-flight chain are concerned. We note that the original expression for $A_2$ given by Nakamura *et al.*[11] includes an additional cutoff parameter, which should in principle be set equal to unity for the random-flight chain. Correspondingly, if we retain terms of $\alpha_R^2$ proportional to $\beta_2$ and $\beta_3$ in addition to those proportional to $n^{1/2}\beta_2$ and $n^{1/2}\beta_3$, it may be given by

$$\alpha_R^2=1+\left(\frac{4}{3}-2n^{-1/2}\right)z-4\pi\left(\frac{3}{2\pi a^2}\right)^3\beta_3+\cdots, \tag{32}$$

where $z$ is the conventional excluded-volume parameter[3] redefined by

$$z=\left(\frac{3}{2\pi a^2}\right)^{3/2}\beta n^{1/2} \tag{33}$$

with the effective binary-cluster integral $\beta$ in place of the (bare) binary cluster integral $\beta_2$. It is seen from Eqs. (30) and (32) that there remain the residual contributions of $\beta_3$ both to $A_2$ and $\alpha_R^2$, the former being proportional to $n^{-1/2}$ ($M^{-1/2}$) and the latter to $n^0$ (constant).

Now, as in the case of the random-flight chain, $A_2$ for the HW chain (composed of $n+1$ identical beads), i.e., $A_2^{(\mathrm{HW})}$ may be expanded in terms of $\beta_2$ and $\beta_3$, the derivation being given in the Appendix. The result reads

$$A_2^{(\mathrm{HW})}=\frac{N_A L^2}{2M^2a^2}\left\{\beta-2\left(\frac{3}{2\pi c_\infty}\right)^{3/2}(\lambda a)^2\left(\frac{\beta_3}{a^3}\right)\times[I(\infty)-I(\lambda L)]+\cdots\right\} \tag{34}$$

with $\beta$ the effective binary-cluster integral redefined by

$$\beta=\beta_2+2\left(\frac{3}{2\pi c_\infty}\right)^{3/2}(\lambda a)^2\left(\frac{\beta_3}{a^3}\right)I(\infty) \tag{35}$$

for the HW chain, where the the function $I(L)$ of (reduced) $L$ is given by

$$\begin{aligned} I(L)&=\exp(-6L^{-1}+0.3472-0.087L) \quad \text{for } 0\leqslant L\leqslant 3.075\\ &=0.4149-0.8027L^{-1}+0.01L^{-1}(7.132\Delta^2-0.9315\Delta^3\\ &\quad +0.1057\Delta^4-0.005\,745\Delta^5) \quad \text{for } 3.075<L<7.075\\ &=1.465-4L^{-1/2}+3.476L^{-1}-\tfrac{5}{6}L^{-3/2} \quad \text{for } 7.075\leqslant L \end{aligned} \tag{36}$$

with $\Delta=L-3.075$. The function $I(L)$ approaches 1.465 and 0 in the limits of $L\to\infty$ and $L\to 0$, respectively, so that the factor $I(\infty)-I(\lambda L)$ on the right-hand side of Eq. (34) becomes $4(\lambda L)^{-1/2}$ in the limit of $\lambda L\to\infty$ and approaches the value 1.465 in the limit of $\lambda L\to 0$. As also derived in the Appendix, the result for $\alpha_R^2$ reads

$$\alpha_R^2=1+K(\lambda L)z-C(\lambda L)\left(\frac{3\lambda}{2\pi c_\infty a}\right)^3\beta_3+\cdots, \tag{37}$$

where $z$ is given by Eq. (20) with Eq. (16) with $\beta$ given by Eq. (35) in place of $\beta_2$, and the coefficient $C(\lambda L)$ as a function of $\lambda L$ approaches a constant independent of $\lambda L$ in the limit of $\lambda L\to\infty$ and vanishes in the limit of $\lambda L\to 0$, although the explicit expression for it is omitted.

From a comparison of Eqs. (34), (35), and (37) for the HW chain with Eqs. (30), (31), and (32) for the random-flight chain, it is seen that the former are essentially the same as the latter except that the residual contribution of $\beta_3$ to $A_2^{(\mathrm{HW})}$ at $\beta=0$ converges to a finite value in the limit of $\lambda L\to 0$ ($M\to 0$), while the corresponding contribution to $A_2$ at $\beta=0$ for the random-flight chain diverges in this limit. For both the HW and random-flight chains, the indication is that even at $\beta=0$, the residual contribution of $\beta_3$ to $A_2$ exists, and moreover, $\alpha_R^2$ takes a value different from unity. However, even within the framework of the present theory which takes account of three-segment interactions, it seems reasonable to consider that the Θ temperature (state) is the temperature at which $\beta$ (instead of $\beta_2$) vanishes. In the remainder of this section, we examine whether the behavior of the residual contributions of $\beta_3$ to $A_2$ and $\alpha_R^2$ in this Θ state is or is not consistent with the usual definition of the Θ temperature that it is the temperature at which $A_2$ vanishes for very large $M$ and also $\langle R^2\rangle/M$ (or $\langle S^2\rangle/M$) becomes there a constant independent of $M$.

Now the residual contribution $A_{2,\Theta}^{(\mathrm{HW})}$ of $\beta_3$ to $A_2^{(\mathrm{HW})}$ given by Eq. (34) at Θ ($\beta=0$) may be written in the form

$$A_{2,\Theta}^{(\mathrm{HW})}=-\frac{3A_3^0(\lambda/M_L)^{1/2}}{8\pi^{3/2}N_A(\langle S^2\rangle_0/M)_\infty^{3/2}}[I(\infty)-I(\lambda L)], \tag{38}$$

where $A_3^0$ is the third virial coefficient for the HW chain composed of $n+1$ identical beads at Θ given by[2,27]

$$A_3^0=\frac{N_A^2 n^3\beta_3}{3M^3}, \tag{39}$$

and $(\langle S^2\rangle_0/M)_\infty$ is the value of $\langle S^2\rangle_0/M$ in the limit of $M\to\infty$. From Eq. (38) with Eq. (36), we have

$$A_{2,\Theta}^{(\mathrm{HW})} = -\frac{3A_3^0}{2\pi^{3/2}N_A(\langle S^2\rangle_0/M)_\infty^{3/2}}M^{-1/2} \quad (\text{for large } M)$$
$$= -\frac{3A_3^0(\lambda/M_L)^{1/2}}{8\pi^{3/2}N_A(\langle S^2\rangle_0/M)_\infty^{3/2}}I(\infty) \quad (\text{for small } M). \tag{40}$$

Thus $A_{2,\Theta}^{(\mathrm{HW})}$ and therefore $A_{2,\Theta}$ vanish for very large $M$.

It is pertinent to make here some remarks. For the random-flight chain, $A_{2,\Theta}$ is given by the right-hand side of the first line of Eqs. (40) over the whole range of $M$ (and diverges in the limit of $M\to 0$), as seen from Eq. (30). The asymptotic form ($\propto M^{-1/2}$) of $A_{2,\Theta}$ in the limit of $M\to\infty$ is therefore independent of chain model, while the coefficients of $\beta_3$ involved in $\beta$ given by Eqs. (35) and (31) for the two chains are differnt from each other, since the factor $I(\infty)$ in Eq. (35) is closely related to the ring-closure probability (see the Appendix). Note that the value 1.465 of $I(\infty)$ for the HW chain is replaced by 2 for the random-flight chain (for which $\lambda a=1$ and $c_\infty=1$), and that the former value obtained by the use of the new version of the ring-closure probability for the KP chain[6] is somewhat smaller than the corresponding value 1.580 obtained by Nakamura *et al.*[11] by the use of its original version[24] (see the Appendix).

It is interesting and important to make an estimate of order of magnitude of $A_{2,\Theta}^{(\mathrm{HW})}$ given by Eq. (38). For this purpose, we evaluate it for the present MC chain at $T_{0-0}^*=3.72$ ($\Theta^*$). The value of $A_3^0$ required for this evaluation is not directly available, so that we estimate it indirectly in the following manner. In the limit of $M\to\infty$, the effects of chain ends disappear and the apparent interpenetration function $\Psi_{\mathrm{ap}}$ defined by Eq. (9) is identical to the (true) interpenetration function $\Psi$. From Eq. (9) with the first line of Eqs. (40), the interpenetration function $\Psi$ at $\Theta$ in the limit of $M\to\infty$, which we denote by $\Psi_{\Theta,\infty}$, may then be written in the form

$$\Psi_{\Theta,\infty} = -\frac{3A_3^0}{8\pi^3N_A^2(\langle S^2\rangle_0/M)_\infty^3} = -\left(\frac{3\lambda}{\pi c_\infty a}\right)^3\beta_3. \tag{41}$$

Thus we can evaluate $A_3^0$ if $\Psi_{\Theta,\infty}$ is known. It is seen from Table II for $\Psi_{\mathrm{ap}}$ at $T_{0-0}^*=3.72$ ($\Theta^*$) that the value of $\Psi_{\mathrm{ap}}$ at $T_{1-1}^*=3.72$ for $n=100-500$ is independent of $n$ within statistical error. We may then adopt as the value of $\Psi_{\Theta,\infty}$ the mean $-0.048_5$ of the three values of $\Psi_{\mathrm{ap}}$ for $n=100$, 200, and 500, and thus as that of $A_3^0$ the value $6.9_7\times10^{-4}$ cm$^6$ mol/g$^3$. The latter has been calculated from the first line of Eqs. (41) with the above-obtained value of $\Psi_{\Theta,\infty}$ and the value $7.8_2\times10^{-18}$ cm$^2$ g/mol of $(\langle S^2\rangle_0/M)_\infty$ calculated from $(\langle S^2\rangle_0/M)_\infty=(6\lambda M_L)^{-1}$ with the values of $\lambda^{-1}$ and $M_L$ given in Sec. III B. The value of $A_3^0$ so evaluated is of the same order of magnitude as the experimental values $4.7\times10^{-4}$ cm$^6$ mol/g$^3$ for $a$-PS in cyclohexane at 34.5 °C ($\Theta$),[27] $4.3\times10^{-4}$ cm$^6$ mol/g$^3$ for $a$-PS in *trans*-decalin at 21.0 °C ($\Theta$), which has been calculated from Eq. (39) with the value $4\times10^{-45}$ cm$^6$ of $\beta_3$ (per repeat unit) obtained by Nakamura *et al.*,[28] and $5.8\times10^{-4}$ cm$^6$ mol/g$^3$ for atactic poly(methyl methacrylate) ($a$-PMMA) in acetonitrile at 44.0 °C ($\Theta$).[27] This indicates that the above estimate of $A_3^0$ from $\Psi_{\mathrm{ap}}$ is reasonable, and also that the present MC model may well describe real systems.

In Fig. 6, the dashed curve represents the theoretical values of $A_{2,\Theta}^{(\mathrm{HW})}$ calculated from Eq. (38) with Eq. (36) with the above-mentioned MC values of $A_3^0$, $(\langle S^2\rangle_0/M)_\infty$, $\lambda^{-1}$, and $M_L$. It is seen that the theoretical values are rather close to the MC values at $T_{1-1}^*=3.72$. The indication is that the present MC chain composed of $n+1$ identical beads at $T_{0-0}^*=\Theta^*$ may be closely identified with the desired fictitious chain at $\Theta$, and that the fact that the residual contribution $A_{2,\Theta}^{(\mathrm{HW})}$ of $\beta_3$ to $A_2^{(\mathrm{HW})}$ remains finite (negative) except for very large $M$ may be accepted.

Next we consider $\alpha_R^2$. At $\Theta$ ($\beta=0$), Eq. (37) becomes

$$\alpha_R^2 = 1 - \frac{3A_3^0C(\lambda L)}{64\pi^3N_A^2(\langle S^2\rangle_0/M)_\infty^3} + \cdots \quad (\text{at } \Theta). \tag{42}$$

We note that $C(\lambda L)\equiv 4\pi$ for the random-flight chain. Since an expression for $C(\lambda L)$ for the HW chain has not explicitly been derived, we estimate the second term on the right-hand side of Eq. (42), i.e., the residual contribution of $\beta_3$ to $\alpha_R^2$ for the random-flight chain. It is evaluated to be 0.102 from the above-mentioned values of $A_3^0$ and $(\langle S^2\rangle_0/M)_\infty$. In the case of the HW chain, for which $C(0)=0$, as mentioned above, the ratio $\langle S^2\rangle_\Theta/M$ of the mean-square radius of gyration to $M$ at $\Theta$ in the limit of $M\to\infty$ may also be about 10% smaller than the corresponding "unperturbed" ratio $\langle S^2\rangle_0/M$ for the ideal chain with the vanishing $\beta_2$ and $\beta_3$. Then, in a practical analysis of experimental data on the basis of the HW chain,[2] such a decrease may be absorbed into the HW model parameters, and an associated increase in the observed expansion factor $\alpha_S$ may be absorbed into the effective binary-cluster integral $\beta$, regarding the decreased dimension $\langle S^2\rangle_0\alpha_S^2$ (at $\Theta$) as the new $\langle S^2\rangle_0=\langle S^2\rangle_\Theta$ for all $M$. Thus the analysis of experimental data made so far for single-chain properties in the QTP scheme[2] is not necessary to change.

In sum, it may be concluded that the effective binary-cluster integral $\beta$ vanishes indeed at the $\Theta$ temperature, and that the dilute solution behavior of polymers may be still explained by the HW theory only if the residual contribution of three-segment interactions to $A_2$ at $\Theta$ is taken into account, i.e., only if Eq. (38) is used instead of the relation, $A_{2,\Theta}^{(\mathrm{HW})}=0$, in the binary cluster approximation. We note that such a contribution may be ignored for good-solvent systems, considering that $\beta_3$ may decrease with increasing solvent power since the third virial coefficient decreases with increasing temperature for gases above the Boyle temperature.[29]

### C. Effects of chain ends

Now we examine the effects of chain ends revealed by the present MC data for $A_2$, following the procedure used in an analysis of experimental data.[2,8] The contribution $A_2^{(E)}$ of the effects to $A_2$ may be estimated by subtracting values of the theoretical $A_2^{(\mathrm{HW})}$ and $A_{2,\Theta}^{(\mathrm{HW})}$ from MC values for $A_2$ shown in Figs. 5 and 6, respectively. As seen from Eq. (27), the theory predicts that $A_2^{(E)}M$ is linear in $M^{-1}$. Thus, if the present MC data are well explained by the theory given in

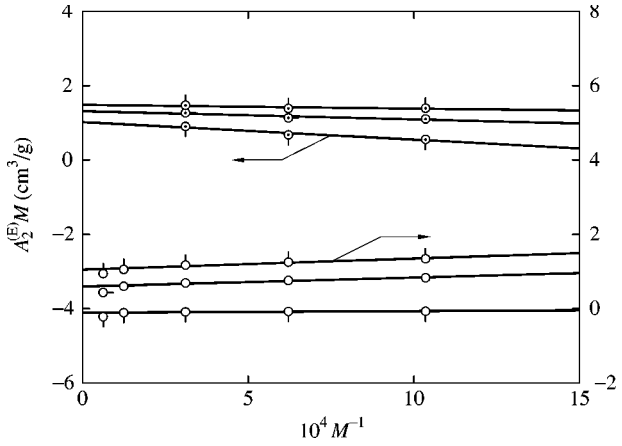


FIG. 7. Plots of $A_2^{(E)}M$ against $M^{-1}$. The symbols have the same meaning as those in Figs. 5 and 6.

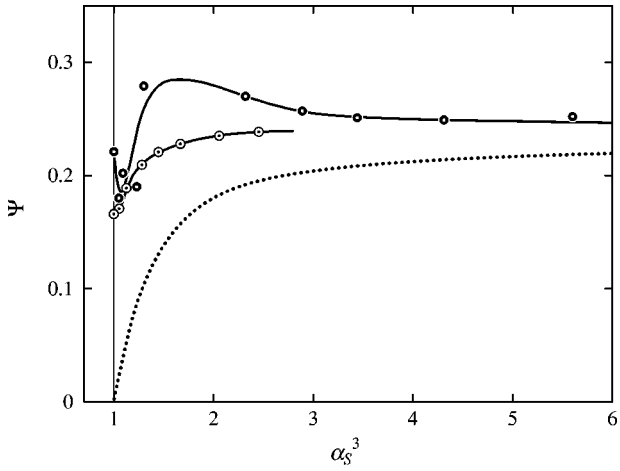


FIG. 8. Plots of $\Psi$ against $\alpha_S{}^3$. The open circles, each with center dot, and the closed circles, each with center hole, represent the present MC values at $T^*_{0-0}=8.0$ and the experimental values for $a$-PS in toluene at 15.0 °C,[8] respectively. The solid curves connect smoothly the respective data points, and the dotted curve represents the TP theory values.

Sec. IV A with $A_{2,\Theta}^{(\mathrm{HW})}$ given by Eq. (38) in place of $A_{2,\Theta}^{(\mathrm{HW})}=0$, then the plot of MC values of $A_2^{(E)}M$ against $M^{-1}$ must follow a straight line.

Figure 7 shows plots of $A_2^{(E)}M$ against $M^{-1}$. The open circles, each with center dot, represent the MC values at $T^*_{0-0}=8.0$ and at $T^*_{1-1}=20.0$ (pip up), $T^*_{1-1}=8.0$ (pip right), and $T^*_{1-1}=3.72$ (pip down) obtained following the above-mentioned procedure with the values in Fig. 5. The theoretical values of $A_2^{(\mathrm{HW})}$ have been calculated from Eq. (14) with the values of $\lambda^{-1}$ and $M_L$ given in Sec. III B and with the value 0.27 of $\lambda B$ evaluated in Paper I[1] for the case of $T^*_{0-0}=8.0$. Recall that $c_\infty=1$ for the present case of the KP chain ($\kappa_0=0$). The open circles represent the MC values at $T^*_{0-0}=3.72$ ($\Theta^*$) and at $T^*_{1-1}=20.0$ (pip up), $T^*_{1-1}=8.0$ (pip right), and $T^*_{1-1}=3.72$ (pip down) obtained similarly with the values in Fig. 6. The theoretical values of $A_{2,\Theta}^{(\mathrm{HW})}$ have been calculated from Eq. (38) with Eq. (36) with the values of $A_3^0$ and $(\langle S^2\rangle_0/M)_\infty$ given in Sec. IV B and also with those of $\lambda^{-1}$ and $M_L$ given in Sec. III B. The data points for each set of $T^*_{0-0}$ and $T^*_{1-1}$ can be fitted by a straight line, and with values of its intercept $a_1$ and slope $a_2$, $\beta_{2,1}$ and $\beta_{2,2}$ may be calculated from Eqs. (28) with Eq. (29). The results so obtained for $\beta_{2,1}$ and $\beta_{2,2}$ taking the repeat unit as a single bond or a single bead (with $M_0=161$) are 200 and 310 Å$^3$ at $T^*_{0-0}=8.0$ and $T^*_{1-1}=20.0$, 180 and 170 Å$^3$ at $T^*_{0-0}=8.0$ and $T^*_{1-1}=8.0$, 140 and $-120$ Å$^3$ at $T^*_{0-0}=8.0$ and $T^*_{1-1}=3.72$, 140 and 530 Å$^3$ at $T^*_{0-0}=3.72$ and $T^*_{1-1}=20.0$, 80 and 360 Å$^3$ at $T^*_{0-0}=3.72$ and $T^*_{1-1}=8.0$, and 14 and 5.7 Å$^3$ at $T^*_{0-0}=3.72$ and $T^*_{1-1}=3.72$, respectively. It is interesting to note that the values of $\beta_{2,1}$ and $\beta_{2,2}$ at $T^*_{0-0}=T^*_{1-1}=3.72$ (for the chain composed of $n+1$ identical beads at $\Theta^*$) are appreciably smaller than those at other reduced temperatures, indicating that the MC chain at $T^*_{0-0}=T^*_{1-1}=3.72$ is very close to the fictitious chain without the effects of chain ends in the range of $n$ studied, as mentioned in the preceding section.

The solid curve in Fig. 6 associated with the MC data points at each $T^*_{1-1}$ represents the theoretical values obtained by adding the values of $A_{2,\Theta}^{(\mathrm{HW})}$ represented by the dashed curve in Fig. 6 to those of $A_2^{(E)}$ calculated from Eq. (27) with the above-determined values of $\beta_{2,1}$ and $\beta_{2,2}$. Agreement between theory and simulation is excellent.

### D. Interpenetration function

Finally, we examine the behavior of the (true) interpenetration function $\Psi$, which is defined for $A_2^{(\mathrm{HW})}$ without the effects of chain ends. Then its MC values should be calculated from

$$\Psi=\frac{A_2^{(\mathrm{HW})}M^2}{4\pi^{3/2}N_A\langle S^2\rangle^{3/2}} \tag{43}$$

with MC values of $A_2^{(\mathrm{HW})}$ obtained from $A_2^{(\mathrm{HW})}=A_2-A_2^{(E)}$ with MC values of $A_2$ and values of $A_2^{(E)}$ calculated from Eq. (27) with the values of $\beta_{2,1}$ and $\beta_{2,2}$ determined in Sec. IV C. Substitution of Eq. (14) into Eq. (43) leads to the corresponding theoretical expression,

$$\Psi=\left(\frac{6\lambda\langle S^2\rangle_0}{c_\infty L}\right)^{-3/2}\bar{z}h(\hat{z}) \tag{44}$$

with

$$\bar{z}=z/\alpha_S^3. \tag{45}$$

Figure 8 shows plots of $\Psi$ against $\alpha_S^3$. The open circles, each with center dot, represent the MC values at $T^*_{0-0}=8.0$. After subtraction of $A_2^{(E)}$, the MC value of $A_2^{(\mathrm{HW})}$ at $T^*_{0-0}=8.0$ becomes almost independent of $T^*_{1-1}$, so that we have shown the data points only at $T^*_{1-1}=8.0$ by the symbols without pip. The value of $\alpha_S^2$ for each data point has been calculated by dividing the value of $\langle S^2\rangle_{l=1}/n$ at $T^*_{0-0}=T^*_{1-1}=8.0$ given in Table III by the value at $T^*_{0-0}=T^*_{1-1}=3.72$ given in Table IV. For comparison, the previous experimental values[8] for $a$-PS in toluene at 15.0 °C are also shown by the closed circles, each with center hole. The solid curves connect smoothly the respective data points, and the dotted curve represents the TP theory values calculated from Eq. (44) with Eqs. (17), (18), (21), and (45) and with the relations $\tilde{z}=\tilde{\bar{z}}=z$ and $6\lambda\langle S^2\rangle_0/c_\infty L=1$. It is seen that as $\alpha_S^3$

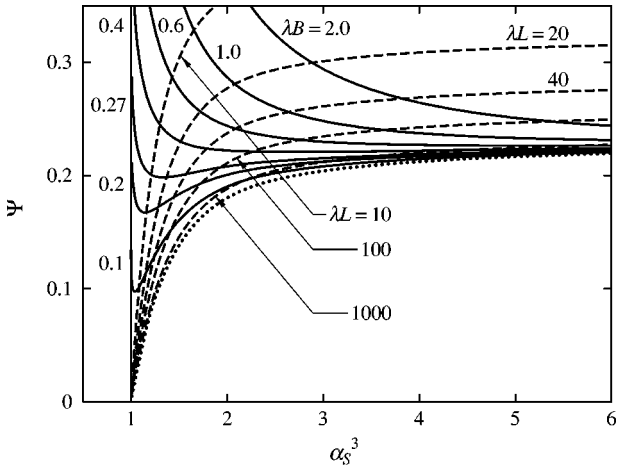


FIG. 9. Plots of the theoretical $\Psi$ against $\alpha_S^3$ for the KP chain. The solid and dashed curves represent the values at constant $\lambda B$ and $\lambda L$, respectively. The dotted curve represents the TP theory values.

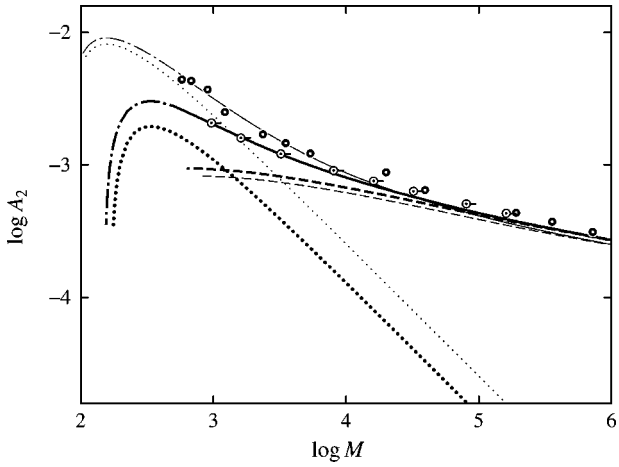


FIG. 10. Double-logarithmic plots of $A_2$ (in $\mathrm{cm^3\,mol/g^2}$) against $M$. The open circles, each with center dot, (pip right) represent the present MC values at $T^*_{0-0}=T^*_{1-1}=8.0$, and the closed circles, each with center hole, the experimental values for $a$-PS in toluene at 15.0 °C (Ref. 8). The solid and dotted–dashed curves represent the theoretical values of $A_2$ $(=A_2^{(\mathrm{HW})}+A_2^{(E)})$, and the dashed and dotted curves those of $A_2^{(\mathrm{HW})}$ and $A_2^{(E)}$, respectively. The heavy and light curves are those for the MC and experimental data points, respectively.

is decreased, $\Psi$ decreases monotonically for the MC chain, while it passes through a maximum and then a minimum for $a$-PS, and that it deviates upward from the TP theory values for both cases. These features arise from the differences in chain stiffness and local chain conformation.

Figure 9 shows similar plots with theoretical values for the KP chain ($\kappa_0=0$). They have been calculated from Eq. (44) with Eqs. (17)–(25) and (45) and with $\langle S^2\rangle_0$ for the KP chain given by

$$\langle S^2\rangle_0=\lambda^{-2}f_{S,\mathrm{KP}}(\lambda L)\quad(\mathrm{KP}),\tag{46}$$

where the function $f_{S,\mathrm{KP}}(L)$ of (reduced) $L$ is given by[30]

$$f_{S,\mathrm{KP}}(L)=\frac{L}{6}-\frac{1}{4}+\frac{1}{4L}-\frac{1}{8L^2}(1-e^{-2L}).\tag{47}$$

The solid curves represent the values for the case in which $\lambda L$ (or $M$) is changed at constant $\lambda B$, while the dashed curves represent the values for the case in which $\lambda B$ is changed at constant $\lambda L$ (or $M$). The dotted curve represents the TP theory values as in Fig. 8. It is seen that the TP theory prediction is obtained as the asymptotic limit of $L\to\infty$ or $B\to 0$, and that for finite $L$ and $B$, $\Psi$ always deviate upward from the TP theory prediction, as observed for the MC and experimental data points shown in Fig. 8. The solid curve for $\lambda B=0.27$ represents the (KP) theoretical values for the MC data points shown in Fig. 8. Agreement between them is rather good except for small $\alpha_S$ (or $M$) as in the case of $\langle S^2\rangle_0$ (see Fig. 4 of Ref. 1). We note that Fig. 9 does not apply to the data points for $a$-PS shown in Fig. 8.

## V. COMPARISON WITH EXPERIMENT

In this section, we further make a comparison of the present MC data with experimental data (with respect to the whole $A_2$).

Figure 10 shows double-logarithmic plots of $A_2$ (in $\mathrm{cm^3\,mol/g^2}$) against $M$. The open circles, each with center dot, (pip right) represent the MC values at $T^*_{0-0}=T^*_{1-1}=8.0$, and the closed circles, each with center hole, the experimental values for $a$-PS in toluene at 15.0 °C.[8] The heavy solid curve represents the (KP) theoretical values calculated for the MC chain from Eqs. (13)–(29) with $\kappa_0=0$, $\lambda^{-1}=16.8$ Å, $M_L=35.8$ $\mathrm{Å^{-1}}$, $\lambda B=0.27$, $\beta_{2,1}=180$ $\mathrm{Å^3}$, and $\beta_{2,2}=170$ $\mathrm{Å^3}$ (for $\lambda L\gtrsim 1$), and the heavy dotted–dashed curve represents those with $h=1$ in Eq. (14) (for $\lambda L\lesssim 1$). (All parameter values used have already been given in Secs. III and IV.) The heavy dashed and dotted curves represent the theoretical contributions of $A_2^{(\mathrm{HW})}$ (for $\lambda L\gtrsim 1$) and $A_2^{(\mathrm{E})}$, respectively, to $A_2$ in Eq. (13). The light curves represent the respective (HW) theoretical values for $a$-PS and have been reproduced from Ref. 2 (or Ref. 8). The dependence of $A_2$ on $M$ for the MC chain at $T^*_{1-1}=8.0$ (and also $T^*_{1-1}=20.0$) may rather be regarded as close to that for $a$-PS in the range of $M$ studied, so that the above-given values of $\beta_{2,1}$ and $\beta_{2,2}$ for the MC chain happen to be of the same order of magnitude as the respective values 220 and 270 $\mathrm{Å^3}$ determined for $a$-PS in toluene.[8] For the MC chain composed of identical beads, the contribution of $A_2^{(E)}$ is appreciably larger at $T^*_{0-0}=T^*_{1-1}=8.0$ than at $T^*_{0-0}=T^*_{1-1}=3.72$ ($\Theta^*$), as seen from Fig. 10. (For the same $\Theta^*$ chain, $A_2^{(E)}$ is very small, as mentioned in Sec. III C.)

Figure 11 shows plots of $A_{2,\Theta}$ against the logarithm of $M$. The open circles represent the MC values at $T^*_{0-0}=3.72$ ($\Theta^*$) and $T^*_{1-1}=8.0$ (pip right) except the one for the largest $M$ at $T^*_{1-1}=3.72$ (pip down). The closed circles, squares, and triangles represent the experimental values for $a$-PS in cyclohexane at 34.5 °C ($\Theta$),[8,31] $a$-PS in *trans*-decalin at 21.0 °C ($\Theta$),[28] and $a$-PMMA in acetonitrile at 44.0 °C ($\Theta$),[32,33] respectively. The solid, dashed, and dotted curves represent the theoretical values for $a$-PS in cyclohexane, $a$-PS in *trans*-decalin, and $a$-PMMA in acetonitrile, respectively, calculated from Eq. (13) with $A_{2,\Theta}^{(\mathrm{HW})}$ given by Eq. (38) with Eq. (36) in place of $A_2^{(\mathrm{HW})}$ and with Eqs. (26)–(29). In the calculation, we have used the values of the HW model parameters $\lambda^{-1}$ (in Å) and $M_L$ (in $\mathrm{Å^{-1}}$), which are 20.6 and

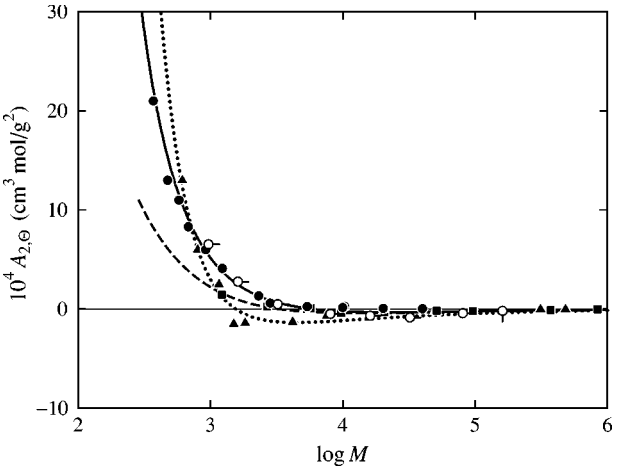


FIG. 11. Plots of $A_{2,\Theta}$ against log $M$. The open circles represent the present MC values at $T^*_{0-0}=3.72$ ($\Theta^*$) and $T^*_{1-1}=8.0$ (pip right) except the one for the largest $M$ at $T^*_{1-1}=3.72$ (pip down), and the closed symbols the experimental values: $a$-PS in cyclohexane at 34.5 °C (circle) (Refs. 8 and 31), $a$-PS in *trans*-decalin at 21.0 °C (square) (Ref. 28), and $a$-PMMA in acetonitrile at 44.0 °C (triangle) (Refs. 32 and 33). The solid, dashed, and dotted curves represent the theoretical values of $A_{2,\Theta}$ ($=A^{(\mathrm{HW})}_{2,\Theta}+A^{(E)}_2$) for $a$-PS in cyclohexane, $a$-PS in *trans*-decalin, and $a$-PMMA in acetonitrile, respectively.

35.8 for $a$-PS[2,34] and 57.9 and 36.3 for $a$-PMMA,[2,35] respectively, and also the literature values of $A^0_3$ (in cm$^6$ mol/g$^3$) and $(\langle S^2\rangle_0/M)_\infty$ (in cm$^2$ mol/g), which are $4.7\times10^{-4}$ and $7.8_2\times10^{-18}$ for $a$-PS in cyclohexane,[27,34] $4.3\times10^{-4}$ and $7.3_9\times10^{-18}$ for $a$-PS in *trans*-decalin,[28] and $5.8\times10^{-4}$ and $6.5_7\times10^{-18}$ for $a$-PMMA in acetonitrile,[27,35] respectively, the $A^0_3$ values having already been given in Sec. VI C. Note that the above values of $\lambda^{-1}$ and $M_L$ for $a$-PS are different from those determined as the KP chain in Sec. III. The values of $\beta_{2,1}$ (in Å$^3$) and $\beta_{2,2}$ (in Å$^3$), which have been determined in the same manner as that in Sec. IV C for the MC chain, are 44 and 200 for $a$-PS in cyclohexane, 31 and 61 for $a$-PS in *trans*-decalin, and $-19$ and 500 for $a$-PMMA in acetonitrile, respectively.

In Fig. 11, all the experimental data points for each system seem to follow closely the corresponding theoretical curve as a whole, although strictly, the data points for $a$-PS in cyclohexane and $a$-PMMA in acetonitrile in the range of $10^4\lesssim M\lesssim10^5$ deviate slightly upward from the respective theoretical curves. The dependence of $A_{2,\Theta}$ on $M$ for the MC chain (at $T^*_{1-1}=8.0$) is close to that for $a$-PS in cyclohexane, so that the respective values 80 and 360 Å$^3$ of $\beta_{2,1}$ and $\beta_{2,2}$ for the former determined in Sec. IV C are of the same order of magnitude as the above-given values for the latter.

## VI. CONCLUSION

We have examined the behavior of the second virial coefficient $A_2$ for polymers by MC simulation of two freely rotating chains with the LJ 6-12 intramolecular and intermolecular potentials between beads in the cutoff version. It has been found that the effects of chain ends on $A_2$ are appreciable for small $M$, as was expected, and that $A_{2,\Theta}$ at the $\Theta$ temperature, at which $\langle S^2\rangle/M$ becomes a constant independent of $M$ for very large $M$, remains slightly negative even for such large (but finite) $M$ where the effects of chain ends disappear. Such behavior of $A_{2,\Theta}$, which cannot be explained within the framework of the binary cluster theory, has been shown to be understandable if possible effects of three-segment interactions are considered. From this finding and also those in a good-solvent condition, it has been concluded that the present MC data for $A_2$ (along with the previous ones for $\langle S^2\rangle$) may be consistently explained as well as experimental data by the theory based on the HW chain model only if the new expression for $A_{2,\Theta}$ derived for the chain with three-segment interctions is used.

## APPENDIX: EFFECTS OF THREE-SEGMENT INTERACTIONS

Following the formulation for the random-flight chain,[3,9] the second virial coefficient $A^{(\mathrm{HW})}_2$ for the HW chain composed of $n+1$ identical beads with the binary and ternary cluster integrals $\beta_2$ and $\beta_3$ may be expanded in the form

$$A^{(\mathrm{HW})}_2=\frac{N_A L^2}{2M^2a^2}\left[\beta_2+2\left(\frac{\beta_3}{a^3}\right)\left(\frac{a}{L}\right)^2\int_0^L ds_1\int_{s_1}^L ds_2\int_0^L ds_3\right.$$
$$\left.\times G(\mathbf{0};s_2-s_1)+\cdots\right], \tag{A1}$$

where $G(\mathbf{0};s)$ is the ring-closure probability for the chain of contour length $s$, i.e., the Green's function $G(\mathbf{R};s)$ representing the distribution of its end-to-end vector distance $\mathbf{R}$ at $\mathbf{R}=\mathbf{0}$.[2] Carrying out integration in the second term on the right-hand side of Eq. (A1) over $s_1$, $s_2$, and $s_3$ with $s_2-s_1$ fixed, we obtain

$$A^{(\mathrm{HW})}_2=\frac{N_A L^2}{2M^2a^2}\left[\beta_2+2\left(\frac{3}{2\pi c_\infty}\right)^{3/2}(\lambda a)^2\right.$$
$$\left.\times\left(\frac{\beta_3}{a^3}\right)I(\lambda L)+\cdots\right], \tag{A2}$$

where the dimensionless factor $I(L)$ as a function of (reduced) $L$ is defined by

$$I(L)=\left(\frac{2\pi c_\infty}{3}\right)^{3/2}\int_0^L\left(1-\frac{s}{L}\right)G(\mathbf{0};s)ds. \tag{A3}$$

We note that $G(\mathbf{0};s)$ in Eq. (A3) is the reduced quantity for which all lengths are measured in units of $\lambda^{-1}$. Considering the fact that (reduced) $G(\mathbf{0};s)$ has the asymptotic form, $(3/2\pi c_\infty)^{3/2}[s^{-3/2}+\mathcal{O}(s^{-5/2})]$, in the limit of $s\to\infty$,[2] $I(L)$ converges to a constant given by

$$I(\infty)=\left(\frac{2\pi c_\infty}{3}\right)^{3/2}\int_0^\infty G(\mathbf{0};s)ds \tag{A4}$$

in the limit of $L\to\infty$, so that Eq. (A2) may be rewritten as Eq. (34).

Similarly, the mean-square end-to-end distance $\langle R^2\rangle$ of the HW chain under consideration may be expanded in the form

$$\langle R^2\rangle=\langle R^2\rangle_0+\left(\frac{\beta_2}{a^2}\right)\int_0^L ds_1\int_{s_1}^L ds_2\left[G(\mathbf{0};s_2-s_1)\langle R^2\rangle_0-\int R^2P_0(\mathbf{R},\mathbf{0}_{s_1s_2};L)d\mathbf{R}\right]$$
$$+\left(\frac{\beta_3}{a^3}\right)\int_0^L ds_1\int_{s_1}^L ds_2\int_{s_2}^L ds_3\left[G(\mathbf{0};s_2-s_1)G(\mathbf{0};s_3-s_2)\langle R^2\rangle_0-\int R^2P_0(\mathbf{R},\mathbf{0}_{s_1s_2},\mathbf{0}_{s_2s_3};L)d\mathbf{R}\right]+\cdots, \quad \text{(A5)}$$

where the subscript 0 refers to the unperturbed value (without excluded volume), the symbol $\mathbf{0}_{s_1s_2}$ means that $\mathbf{R}_{s_1s_2}=\mathbf{0}$, $P_0(\mathbf{R},\mathbf{R}_{s_1s_2};L)$ is the (unperturbed) distribution function of $\mathbf{R}$ $(=\mathbf{R}_{0L})$ and $\mathbf{R}_{s_1s_2}$ for the chain of contour length $L$, and so on with $\mathbf{R}_{s_1s_2}$ being the vector distance between the contour points $s_1$ and $s_2$. The squared end-distance expansion factor $\alpha_R^2$ may then be given, from Eq. (A5), by

$$\alpha_R^2=1+K(\lambda L)\left(\frac{3}{2\pi c_\infty}\right)^{3/2}\left(\frac{\lambda\beta_2}{a^2}\right)(\lambda L)^{1/2}$$
$$+K_3(\lambda L)\left(\frac{3}{2\pi c_\infty}\right)^3\left(\frac{\lambda^3\beta_3}{a^3}\right)(\lambda L)^{1/2}+\cdots, \quad \text{(A6)}$$

where $K(L)$ and $K_3(L)$ are the dimensionless coefficients as functions of (reduced) $L$, the former being given by Eq. (23) and the latter by

$$K_3(L)=\left(\frac{2\pi c_\infty}{3}\right)^3 L^{-1/2}\langle R^2\rangle_0^{-1}\int_0^L ds_1\int_{s_1}^L ds_2\int_{s_2}^L ds_3$$
$$\times\left\{c_\infty(s_3-s_1)\,G(\mathbf{0};s_2-s_1)G(\mathbf{0};s_3-s_2)-(c_\infty L-\langle R^2\rangle_0)G(\mathbf{0};s_2-s_1)G(\mathbf{0};s_3-s_2)\right.$$
$$\left.-\left[\int R^2P_0(\mathbf{R},\mathbf{0}_{s_1s_2},\mathbf{0}_{s_2s_3};L)d\mathbf{R}-c_\infty(L-s_3+s_1)G(\mathbf{0};s_2-s_1)G(\mathbf{0};s_3-s_2)\right]\right\}. \quad \text{(A8)}$$

Considering the facts that $G(\mathbf{0};s)$ has the above-mentioned asymptotic form in the limit of $s\to\infty$, that $\langle R^2\rangle_0$ becomes $c_\infty L$ in the limit of $L\to\infty$,[2] and that $\int R^2P_0(\mathbf{R},\mathbf{0}_{s_1s_2},\mathbf{0}_{s_2s_3};L)d\mathbf{R}$ becomes $c_\infty[L-(s_3-s_1)]G(\mathbf{0};s_2-s_1)G(\mathbf{0};s_3-s_2)$ in the limit of $L-(s_3-s_1)\to\infty$, it can be shown that the coil-limiting value arises only from the first term in curly brackets on the right-hand side of Eq. (A8), so that the symptotic form of $K_3(L)$ may be given by

$$K_3(L)=2[L^{-1/2}f_1(L)-L^{-3/2}f_2(L)]+\mathcal{O}(L^{-1/2}), \quad \text{(A9)}$$

where $f_1(L)$ and $f_2(L)$ are given by

$$K_3(L)=\left(\frac{2\pi c_\infty}{3}\right)^3 L^{-1/2}\langle R^2\rangle_0^{-1}\int_0^L ds_1\int_{s_1}^L ds_2\int_{s_2}^L ds_3$$
$$\times\left[G(\mathbf{0};s_2-s_1)G(\mathbf{0};s_3-s_2)\langle R^2\rangle_0\right.$$
$$\left.-\int R^2\,P_0(\mathbf{R},\mathbf{0}_{s_1s_2},\mathbf{0}_{s_2s_3};L)d\mathbf{R}\right]. \quad \text{(A7)}$$

In Eq. (A7) and in what follows, all lengths are measured in units of $\lambda^{-1}$ unless otherwise noted, for simplicity. The coefficient $K_3(L)$ should converge to a constant independent of $L$ in the limit of $L\to\infty$. If it did not, the third term on the right-hand side of Eq. (A6), which represents the contribution of three-segment interactions, would diverge faster than the second. We note that $K_3(L)$ vanishes in the limit of $L\to 0$, since $G(\mathbf{0};s)$ converges to 0 in the limit of $s\to 0$ faster than $s^m$ and since $P_0(\mathbf{R},\mathbf{0}_{s_1s_2},\mathbf{0}_{s_2s_3};L)$ converges to 0 in the limit of $|s_2-s_1|\to 0$ (or $|s_3-s_2|\to 0$) faster than $|s_2-s_1|^n$ (or $|s_3-s_2|^n$), where $m$ and $n$ are arbitrary positive integers.

The coil-limiting value of $K_3(L)$ in the limit of $L\to\infty$ may be evaluated as follows. Equation (A7) may be rewritten in the form

$$f_1(L)=\left(\frac{2\pi c_\infty}{3}\right)^3\int_0^L ds_1\,s_1\,G(\mathbf{0};s_1)\int_0^{L-s_1}ds_2\,G(\mathbf{0};s_2), \quad \text{(A10)}$$

$$f_2(L)=\left(\frac{2\pi c_\infty}{3}\right)^3\int_0^L ds_1\,s_1^2\,G(\mathbf{0};s_1)\int_0^{L-s_1}ds_2\,G(\mathbf{0};s_2). \quad \text{(A11)}$$

The respective Laplace transforms $\tilde{f}_1(p)$ and $\tilde{f}_2(p)$ of $f_1(L)$ and $f_2(L)$ in the vicinity of $p=0$ may be given by

$$\tilde{f}_1(p)=\pi^{1/2}\left(\frac{2\pi c_\infty}{3}\right)^{3/2}\tilde{G}(\mathbf{0};0)p^{-3/2}, \quad \text{(A12)}$$

$$\tilde{f}_2(p)=\frac{\pi^{1/2}}{2}\left(\frac{2\pi c_\infty}{3}\right)^{3/2}\tilde{G}(\mathbf{0};0)p^{-5/2}, \tag{A13}$$

where $\tilde{G}(\mathbf{0};0)$ is the Laplace transform $\tilde{G}(\mathbf{0};p)$ of $G(\mathbf{0};s)$ at $p=0$ and is given by

$$\tilde{G}(\mathbf{0};0)=\int_0^\infty G(\mathbf{0};s)ds=\left(\frac{3}{2\pi c_\infty}\right)^{3/2}I(\infty). \tag{A14}$$

Substitution of $f_1(L)$ and $f_2(L)$ obtained by Laplace inversion of $\tilde{f}_1(p)$ and $\tilde{f}_2(p)$, respectively, into Eq. (A9) leads to

$$K_3(L)=\tfrac{8}{3}I(\infty)+\mathcal{O}(L^{-1/2}). \tag{A15}$$

From Eq. (A6) with Eq. (A15), we obtain Eq. (37), where the dimensionless coefficient $C(L)$ as a function of (reduced) $L$ is defined by

$$C(L)=L^{1/2}[2I(\infty)K(L)-K_3(L)]. \tag{A16}$$

We note that $C(L)$ approaches a constant independent of $L$ in the limit of $L\to\infty$ and vanishes in the limit of $L\to 0$.

Finally, for practical use, we construct an approximate formula for the factor $I(L)$ given by Eq. (A3), assuming the approximate expession for $G(\mathbf{0};s)$ for the KP chain given by[6]

$$\begin{aligned}G(\mathbf{0};s)&=28.01s^{-5}\exp(-7.027s^{-1}+0.492s) \quad \text{for } 0\leqslant s\leqslant 3.075\\ &=0.01(4.706-1.844\Delta+0.4185\Delta^2-0.03791\Delta^3) \quad \text{for } 3.075<s<7.075\\ &=\left(\frac{3}{2\pi s}\right)^{3/2}\left(1-\frac{5}{8}s^{-1}\right) \quad \text{for } 7.075\leqslant s\end{aligned} \tag{A17}$$

with $\Delta=s-3.075$ as in the case of $K(L)$. (This assumption has been justified.[2,6]) With values of $I(L)$ obtained by numerical integration of $G(\mathbf{0};s)$ and $sG(\mathbf{0};s)$ for $0\leqslant L\leqslant 3.075$, we have constructed the desired formula, Eq. (36). We note that the error in the value of $I(\infty)-I(L)$ calculated from Eq. (36) in the range of $0\leqslant L\leqslant 3.075$ does not exceed 0.15%.

[1] H. Yamakawa and T. Yoshizaki, J. Chem. Phys. **118**, 2911 (2003).
[2] H. Yamakawa, *Helical Wormlike Chains in Polymer Solutions* (Springer, Berlin, 1997).
[3] H. Yamakawa, *Modern Theory of Polymer Solutions* (Harper & Row, New York, 1971), its electronic edition is available on-line at the URL: http://www.molsci.polym.kyoto-u.ac.jp/archives/redbook.pdf
[4] J. P. Hansen and I. R. McDonald, *Theory of Simple Liquids*, 2nd ed. (Academic, London, 1986).
[5] H. Yamakawa and J. Shimada, J. Chem. Phys. **83**, 2607 (1985).
[6] J. Shimada and H. Yamakawa, J. Chem. Phys. **85**, 591 (1986).
[7] H. Yamakawa, Macromolecules **25**, 1912 (1992).
[8] Y. Einaga, F. Abe, and H. Yamakawa, Macromolecules **26**, 6243 (1993).
[9] H. Yamakawa, J. Chem. Phys. **45**, 2606 (1966).
[10] B. J. Cherayil, J. F. Douglas, and K. F. Freed, J. Chem. Phys. **83**, 5293 (1985).
[11] Y. Nakamura, T. Norisuye, and A. Teramoto, Macromolecules **24**, 4904 (1991).
[12] W. G. McMillan and J. E. Mayer, J. Chem. Phys. **13**, 276 (1945).
[13] V. I. Harismiadis and I. Szleifer, Mol. Phys. **81**, 851 (1994).
[14] J. Dautenhahn and C. K. Hall, Macromolecules **27**, 5399 (1994).
[15] P. G. Bolhuis, A. A. Louis, J. P. Hansen, and E. J. Meijer, J. Chem. Phys. **114**, 4296 (2001).
[16] S. D. Stellman and P. J. Gans, Macromolecules **5**, 516 (1972).
[17] S. D. Stellman, M. Froimowitz, and P. J. Gans, J. Comput. Phys. **7**, 178 (1971).
[18] M. Matsumoto and T. Nishimura, ACM Trans. Model. Comput. Simul. **8**, 3 (1998), see also the URL: http://www.math.keio.ac.jp/matumoto/emt.html
[19] O. F. Olaj, B. Neubauer, and G. Zifferer, Macromolecules **31**, 4342 (1998).
[20] O. Kratky and G. Porod, Recl. Trav. Chim. Pays-Bas **68**, 1106 (1949).
[21] T. Konishi, T. Yoshizaki, T. Saito, Y. Einaga, and H. Yamakawa, Macromolecules **23**, 290 (1990).
[22] T. Konishi, T. Yoshizaki, and H. Yamakawa, Macromolecules **24**, 5614 (1991).
[23] W. Bruns, Macromolecules **22**, 2829 (1989).
[24] H. Yamakawa and W. H. Stockmayer, J. Chem. Phys. **57**, 2843 (1972).
[25] C. Domb and A. J. Barrett, Polymer **17**, 179 (1976).
[26] P.-G. de Gennes, *Scaling Concepts in Polymer Physics* (Cornell University, Ithaca, NY, 1979).
[27] H. Yamakawa, F. Abe, and Y. Einaga, Macromolecules **27**, 3272 (1994).
[28] Y. Nakamura, N. Inoue, T. Norisuye, and A. Teramoto, Macromolecules **30**, 631 (1997).
[29] D. A. McQuarrie, *Statistical Mechanics* (Harper & Row, New York, 1973).
[30] H. Benoit and P. Doty, J. Phys. Chem. **57**, 958 (1953).
[31] H. Yamakawa, F. Abe, and Y. Einaga, Macromolecules **27**, 5704 (1994).
[32] F. Abe, Y. Einaga, and H. Yamakawa, Macromolecules **27**, 3262 (1994).
[33] F. Abe, Y. Einaga, and H. Yamakawa, Macromolecules **28**, 694 (1995).
[34] F. Abe, Y. Einaga, T. Yoshizaki, and H. Yamakawa, Macromolecules **26**, 1884 (1993).
[35] Y. Tamai, T. Konishi, Y. Einaga, M. Fujii, and H. Yamakawa, Macromolecules **23**, 4068 (1990).